

## Synergetic effect on methylene blue adsorption to biochar with gentian violet in dyeing and printing wastewater under competitive adsorption mechanism

Qicheng Chen<sup>a</sup>, Qiaomu Zhang<sup>a</sup>, Yang Yang<sup>b</sup>, Qingyan Wang<sup>a</sup>, Yifeng He<sup>c,\*</sup>, Nanhong Dong<sup>a,\*\*</sup>

<sup>a</sup> School of Energy and Power Engineering, Northeast Electric Power University, Jilin 132012, China

<sup>b</sup> EBRI, Aston University, Birmingham, B4 7ET, UK

<sup>c</sup> College of Forestry, Henan Agricultural University, Zhengzhou 450002, China

### HIGHLIGHTS

- Competitive adsorption of methylene blue and gentian violet from solution was probed firstly.
- Activated carbon obtained by torrefied cornstalk was used as an adsorbent.
- Adsorption kinetics was fitted by pseudo-first- and pseudo-second-order models.
- Competitive adsorption was fitted by Freundlich and Langmuir isotherms.
- Competitive adsorption mechanism and related factors of influence were elucidated.

### ARTICLE INFO

#### Keywords:

Biomass-derived activated carbon  
Kinetics  
Isotherm  
Dye  
Wastewater

### ABSTRACT

Decolorization of dyeing/printing wastewater by carbon-based materials has been carried out to study the adsorption of dye molecules onto adsorbent. Biomass-derived activated carbon (SAC) was sampled from cornstalk pyrolysis in the presence of  $K_2CO_3$  as an activator. Adsorption of methylene blue (MB) and gentian violet (GV) onto SAC was examined to probe the mechanisms, isotherms, and kinetics of dye removal in single- or two-component systems. According to the adsorption rate in a single-component system, three stages were identified. The equilibrium adsorption capacity for MB onto SAC in the single-component system is  $274.84 \text{ mg g}^{-1}$  which is higher than that for GV of  $266.57$ , meanwhile the pseudo-second-order (PSO) model would describe the adsorption kinetics with the correlation coefficient higher than  $0.99$ . In the binary GV-MB system, presence of GV promoted MB adsorption to  $325.15 \text{ mg g}^{-1}$  and  $287.73 \text{ mg g}^{-1}$  at different GV concentrations while the PSO model was also applicable. Furthermore, differences between experimental and calculated values by the Freundlich and Langmuir isotherms indicated the occurrence of competitive adsorption in the two-component system. The gained insights are beneficial for removing the multiple dyes from industrial wastewater, economically and effectively and thus paving the way to the establishment of a greener society.

\* Corresponding author.

\*\* Corresponding author.

E-mail addresses: [heyifeng310@163.com](mailto:heyifeng310@163.com) (Y. He), [N.H.Dong@neepu.edu.cn](mailto:N.H.Dong@neepu.edu.cn) (N. Dong).

<https://doi.org/10.1016/j.csite.2021.101099>

Received 12 March 2021; Received in revised form 8 May 2021; Accepted 22 May 2021

Available online 28 May 2021

2214-157X/© 2021 The Authors. Published by Elsevier Ltd. This is an open access article under the CC BY-NC-ND license

(<http://creativecommons.org/licenses/by-nc-nd/4.0/>).

## 1. Introduction

Organic dyes present in wastewater from textile, dyeing, and leather industries are harmful to the environment and have a devastating impact on ecosystems [1]. For instance, gentian violet (GV) causes skin damage and even cancer in humans and other animals [2–4], while methylene blue (MB) leads to intoxication and insanity (when absorbed through the digestive system) or blindness (upon direct contact with eyes) [5]. Therefore, the pre-discharge treatment of industrial wastewater to remove organic dyes is a task of high importance. Various approaches have been employed to achieve this goal, e.g., ion exchange, chemical oxidation, electrochemical treatment, ozonation, and adsorption [6–8], with adsorption methods being particularly promising because of their high removal rate [9–11].

Biomass is a kind of renewable resource and can be transformed into fuels through thermochemical [12] or biochemical [13] conversion to achieve pollution-free and Carbon-neutral during the combustion [14]. Biomass-derived activated carbon was also employed into the industrial purification of solid waste [15]. Compared to other types of activated carbon, biochar-based materials hold great promise due to the abundance and low cost of their precursors [16] and have been produced from agricultural organic waste such as Thiruvottukai shells [17], ginger roots [18], black sapote seeds [19], white beans [20], coffee beans hush [21], and coal nut shells [22]. A study of the specific surface area of the solid products of variable-temperature biomass roasting [23] showed that in all cases, the highest specific surface area was obtained when roasting was performed at 250 °C in N<sub>2</sub>. Another work probed the formation of gaseous, liquid, and solid products during biomass pyrolysis at 260 °C and different water vapor concentrations for different times, revealing that high water vapor levels benefitted the formation of gaseous and liquid products [24]. Compared with physical activation, chemical activation significantly improves the surface properties of biochar, e.g., leather-based activated carbon prepared by activation with CaCO<sub>3</sub> or KOH had large BET surface areas of 249.93 and 2247.45 m<sup>2</sup> g<sup>-1</sup>, respectively [25].

Dye adsorption in single-component systems has been extensively studied, e.g., a kinetic study of MB or methyl violet adsorption onto wood sawdust indicated that adsorption kinetics is matched to a pseudo-second-order (PSO) model [26]. A carbon-magnetic composite was demonstrated to well adsorb GV, with the adsorption capacity depending on the initial GV concentration [27]. Another study probed the adsorption of Congo red by Fe<sub>x</sub>Co<sub>3-x</sub>O<sub>4</sub> nanoparticles and the intraparticle diffusion could be described by a rate-limiting step [28]. An investigation of the simultaneous adsorption of malachite green and sunset yellow onto Cd(OH)<sub>2</sub>-activated carbon showed that initial concentration and pH determined the dye adsorption ability, obviously [29]. The research on the adsorption of dye molecules onto activated carbon in the multiple-component aqueous system was rarely reported and adsorption mechanism of a single type of dye molecule may not represent the co-existence of multiple dye molecules in dye-contaminated wastewater properly.

By 2018, dyeing wastewater disposal of China was up to 2.3 billion tons per year and water was contaminated by various organic dye molecules. Herein, by considering the absence on the studies of the competitive adsorption mechanism in a binary component system, we emphasized the simultaneous removal of GV and MB in the dyeing and printing wastewater onto straw activated carbon (SAC) which was derived from cornstalk (raw material) and activated by K<sub>2</sub>CO<sub>3</sub> (activator).

## 2. Experimental section

### 2.1. Sample preparation

Raw cornstalk was crushed and sieved through a 150-mesh sieve. Then, 20-g cornstalk samples were loaded into a tube furnace (GS1200-150, Ya Ge Long, China), heated in N<sub>2</sub> to 300 °C at 4 °C min<sup>-1</sup>, and cooled after 1-h torrefaction at 300 °C. Following by rinsing in deionized water three times, the solid residues were well dried and mixed with K<sub>2</sub>CO<sub>3</sub> in a ratio of 1:1.6. After reloading into the tube furnace, the prepared mixtures were baked in N<sub>2</sub> at the heating rate of 10 °C min<sup>-1</sup> to 780 °C and then staying for 1 h before cooling. The collected solids were neutralized with 0.1 M aqueous HCl, rinsed in deionized water and dried to afford SAC samples that were sealed and stored.

### 2.2. Adsorption experiments in single-component systems

A 250-mL conical flask was charged with 100 mL aqueous MB (40 mg L<sup>-1</sup>) and 10 mg SAC, mounted on a shaker (TS-100B, Chuan Yi, China), and shaken for 3–240 min at 180 rpm and 30 °C. Subsequently, the filtration process was carried out to remove the solids and the MB concentration in the filtrate was calculated from its absorbance determined using a spectrophotometer (757, Jing Ke, China). An identical procedure was used for aqueous GV preparation.

In Weber and Morris model [28], the time-dependent intraparticle adsorption can be described as a diffusion-controlled process when its kinetics is interpreted based on the diffusion rate of adsorbate to adsorbent as following:

$$q_t = kt^{0.5} + C \quad (1)$$

where  $C$  is a constant (mg g<sup>-1</sup>),  $q_t$  denotes the time-dependent adsorption capacity (mg g<sup>-1</sup>),  $k$  denotes the intraparticle diffusion rate constant (mg g<sup>-1</sup> min<sup>-0.5</sup>). For this analysis,  $q_t$  is plotted against  $t^{0.5}$ , and  $k$  is obtained as the slope of this plot.

Under equilibrium conditions, the per-unit-mass adsorption capacity of SAC for GV and MB is given as:

$$q_t = V(C_0 - C_1)/m \quad (2)$$

where  $V$  is the solution volume (L),  $C_0$  is the initial dye concentration in wastewater and  $C_1$  is the instantaneous concentration at

different time ( $\text{mg L}^{-1}$ ), and  $m$  denotes the mass of adsorbent (g).

2.3. Adsorption experiments in two-component systems

The simultaneous adsorption of GV and MB onto SAC was probed in the conical flask using [MB ( $40 \text{ mg L}^{-1}$ )+GV ( $10 \text{ mg L}^{-1}$ )], [MB ( $40 \text{ mg L}^{-1}$ )+GV ( $20 \text{ mg L}^{-1}$ )], [MB ( $10 \text{ mg L}^{-1}$ )+GV ( $40 \text{ mg L}^{-1}$ )], and [MB ( $20 \text{ mg L}^{-1}$ )+GV ( $40 \text{ mg L}^{-1}$ )] samples. The flask was sequentially charged with a 100-mL sample and SAC (10 mg) and then shaken on the shaker. After a certain time, the filtrate and SAC were collected for analysis, and the results were fitted with pseudo-first-order (PFO) and pseudo-second-order models [30]. The former model is given by

$$\log(q_e - q_t) = \log q_e - t(k_1 / 2.303) \tag{3}$$

where  $q_e$  is the amount of dye adsorbed at equilibrium ( $\text{mg g}^{-1}$ ), and  $k_1$  denotes the PFO rate constant ( $\text{min}^{-1}$ ). The PSO model can be described by

$$q_t^{-1}t = (k_2q_e^2)^{-1} + q_e^{-1}t \tag{4}$$

where  $k_2$  denotes the equilibrium rate constant ( $\text{g mol}^{-1} \text{min}^{-1}$ ).

2.4. Isotherm experiments

GV solutions were prepared at the concentrations of 10, 20, 30, 40, and 60  $\text{mg L}^{-1}$  and blended with MB solution ( $10 \text{ mg L}^{-1}$ ). A conical flask was sequentially charged with the test solution (100 mL) and SAC (10 mg) and shaken on a shaker for 4 h. Subsequent analysis was performed as described in section 2.2. The obtained data were fitted using Langmuir [31] and Freundlich [32] models.

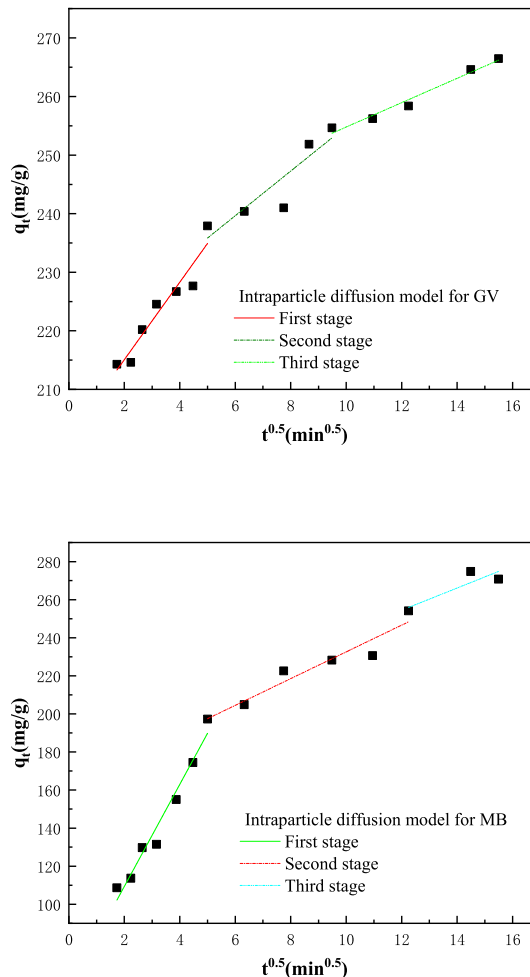


Fig. 1. Intraparticle diffusion model plot for the adsorption of GV and MB onto SAC.

The former model is described by

$$C_e q_e^{-1} = (K_L q_m)^{-1} + C_e q_m^{-1} \tag{5}$$

where  $q_m$  represents the maximum adsorption capacity,  $K_L$  denotes the constant energy depending on the adsorption heat, and  $C_e$  denotes the adsorbate concentration at equilibrium ( $\text{mg L}^{-1}$ ). The Freundlich model is introduced as

$$\ln q_e = \ln K_F + n^{-1} \ln C_e \tag{6}$$

where  $K_F$  is the Freundlich constant ( $\text{mg g}^{-1}$ ), and  $n$  denotes a parameter reflecting adsorption intensity ( $\text{L mg}^{-1}$ ).

### 3. Results and discussion

#### 3.1. Adsorption mechanism

Adsorption in single-component systems was described using intraparticle diffusion dynamics, with the obtained  $q_t$  vs.  $t^{0.5}$  plots provided in Fig. 1. According to the simulated curves, three stages could be identified [33] while the slopes of the corresponding linear portions ( $K_1$ ,  $K_2$ , and  $K_3$ ) were used to evaluate adsorption rate. Ofomaja was trying to present the plots by a single curve, but failed to depict the relationship accurately [34]. In the three-stage description, two periods, namely those before and after 3 min, were further specified in the first stage. In the former period, more GV molecules accumulated on the SAC surface, with GV and MB adsorption amounts of 214.3 and 108.6  $\text{mg g}^{-1}$  at the time of 3 min, respectively. Given the same initial concentrations of these cationic dyes, the

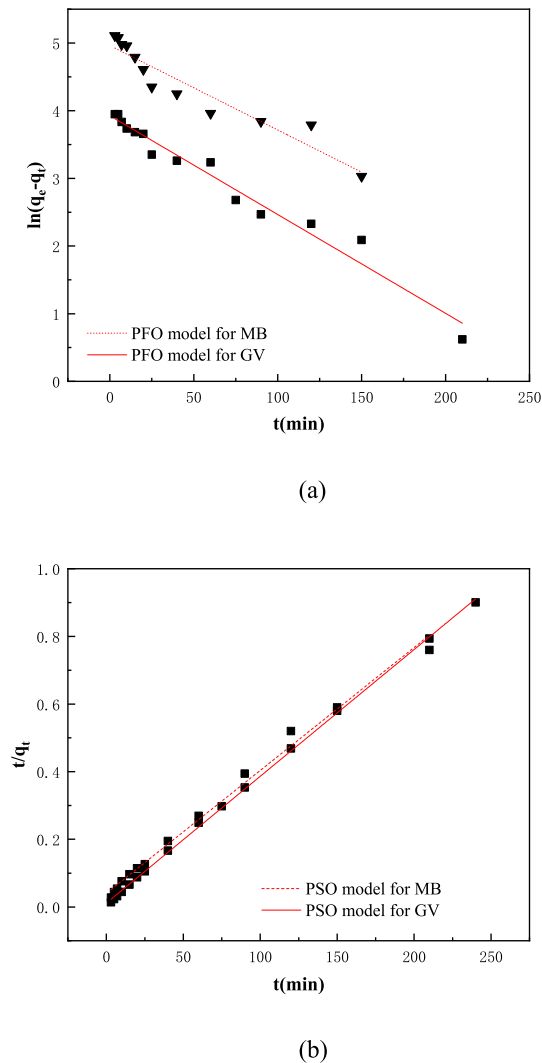


Fig. 2. PFO and PSO models plot for the adsorption of GV and MB onto SAC in single-component system.

above variation was attributed to differences in polar interactions. In particular, GV had a higher ionizability, molecular diameter (1.31 vs. 1.09 nm), and molar mass (407.98 vs. 319.85 g mol<sup>-1</sup>) than MB, thus engaging in a stronger polar interaction with SAC and being more rapidly adsorbed. Hence, in the initial period of the first stage, adsorption behavior was mostly determined by the polarity effect. In the second period, the amount of adsorbed GV increased by 23.6 mg g<sup>-1</sup>, while that of MB increased by 88.7 mg g<sup>-1</sup>. During this period, MB molecules moved toward the SAC surface faster than GV ones, i.e., the rate of concentration decrease in solution was faster for MB, as reflected by the higher  $K_1$  value obtained for the latter dye. This result was ascribed to film or surface diffusion which describes the dye transport from the solution to the adsorbent external surface. The larger intercept value,  $C$  in the second period indicates the rate-limiting step is dominated by the surface diffusion. Moreover, the higher intercept value of GV compared to that of MB shows that surface diffusion was more significant for the absorption of the former dye.

The second stage suggests that the dyes diffused into SAC meso- and micro-pores by pore filling or pore diffusion and can be regarded as a transition stage, with the rate of adsorption determined by that of intraparticle diffusion. Considering the larger molecular size of GV, the diffusion depth of GV in SAC meso- and micro-pores was small and the diffusion rate was slow, in line with the steeper slope of the MB fitting curve in the second stage.

The last stage depicts dye adsorption on adsorbent interior sites. After entering the meso- and micro-pores, the dye molecules were adsorbed at active sites via ion exchange during chemisorption. Then, the stage was dominated by physisorption until adsorption equilibrium was reached. The instability of physisorption resulted in MB desorption after 210 min, while GV was still in a state of slow adsorption at 240 min, which indicated that MB completed the physisorption process to reach adsorption equilibrium faster than GV. As shown in Fig. 1,  $K_1$  reflects the diffusion rate under the effect of polarity and concentration difference,  $K_2$  reflects the intraparticle diffusion rate, and  $K_3$  reflects the rate of chemisorption and physisorption. In this case,  $K_3$  was much smaller than  $K_1$  and  $K_2$ , i.e., chemi-/physisorption was the rate-limiting step.

### 3.2. Kinetic study

#### 3.2.1. Adsorption kinetics in single-component systems

Fig. 2(a) presents  $\log(q_e - q_t)$  vs.  $t$  plots used to obtain the parameters of PFO adsorption kinetics.  $K_1$ , the PFO rate constant was calculated from the slope of fitted straight-line, and  $q_{e,cal}$ , the equilibrium adsorption capacity derived from the corresponding intercept. Fig. 2(b) presents  $t/q_t$  vs.  $t$  plots for MB and GV as well as the fitted straight-line based on the PSO model [35]. The relevant results reveal that chemisorption is the rate-limiting factor. In this case,  $q_{e,cal}$  derived from the reciprocal of the slopes, while  $K_2$  was calculated from the corresponding intercept. Table 1 lists the parameters of MB/GV adsorption onto SAC, demonstrating that the correlation coefficients ( $R^2$ ) of the PSO model for MB and GV sorption equaled 0.9981 and 0.9995, respectively. The discrepancy between  $q_{e,exp}$  (experimental equilibrium adsorption capacity) and  $q_{e,cal}$  of the PFO model equaled 131.93 and 215.84 mg g<sup>-1</sup> for MB and GV, respectively, whereas the corresponding values for the PSO model equaled only 2.98 and 3.74 mg g<sup>-1</sup>, respectively. Meanwhile,  $R^2$  of the PSO model exceeded 0.99 which illustrated that the PSO model well described the experimental findings. It is in consistence with the reported results which indicated that the PSO model can be employed to describe the adsorption kinetics of various dye molecules [36].

#### 3.3. Adsorption kinetics in two-component systems

Curves in Fig. 3 describe the simultaneous adsorption of MB and GV in the solutions onto SAC, with the extracted kinetic parameters listed in Table 2. In the case of the [10 mg L<sup>-1</sup> MB + 40 mg L<sup>-1</sup> GV] system,  $R^2$  values of 0.9895 and 0.9999 were achieved for MB adsorption described by the PFO and PSO models, respectively. When the concentration of MB increased to 40 mg L<sup>-1</sup> and that of GV decreased to 20 or 10 mg L<sup>-1</sup>,  $R^2$  values of 0.9295 and 0.9335 were obtained for MB adsorption corresponding to the PFO model. Although both the correlation coefficients exceeded 0.92, the value of  $q_{e,cal}$  varied obviously to that of

$q_{e,exp}$ . Furthermore, the negative value of  $K_1$  means the PFO model cannot adequately describe GV adsorption. However, MB and GV adsorption could be well represented by the PSO model, as reflected by the satisfied  $R^2$  values and better consistency between  $q_{e,cal}$  and  $q_{e,exp}$ . Thus, the PSO model is supposed to well represent the dye adsorption kinetics of MB and/or GV onto SAC in both single- and two-component systems.

#### 3.4. Adsorption isotherms

Several assumptions by Langmuir isotherm [31]: (i) maximum ion exchange determined by the monolayer saturation level of adsorbate molecules onto the homogeneous adsorbent surface, (ii) a constant power of ion exchange, and (iii) the absence of adsorbate

**Table 1**  
Adsorption kinetic parameters in single-component system.

Samples	$q_{e,exp}$ (mg g <sup>-1</sup> )	PFO			PSO		
		$k_1$ (min <sup>-1</sup> )	$q_{e,cal}$ (mg g <sup>-1</sup> )	$R^2$	$k_2$ (g mg <sup>-1</sup> min <sup>-1</sup> )	$q_{e,cal}$ (mg g <sup>-1</sup> )	$R^2$
MB	274.84	0.0288	142.91	0.9101	$0.32 \times 10^{-3}$	277.82	0.9981
GV	266.57	0.0336	50.73	0.9694	$1.19 \times 10^{-3}$	270.31	0.9995

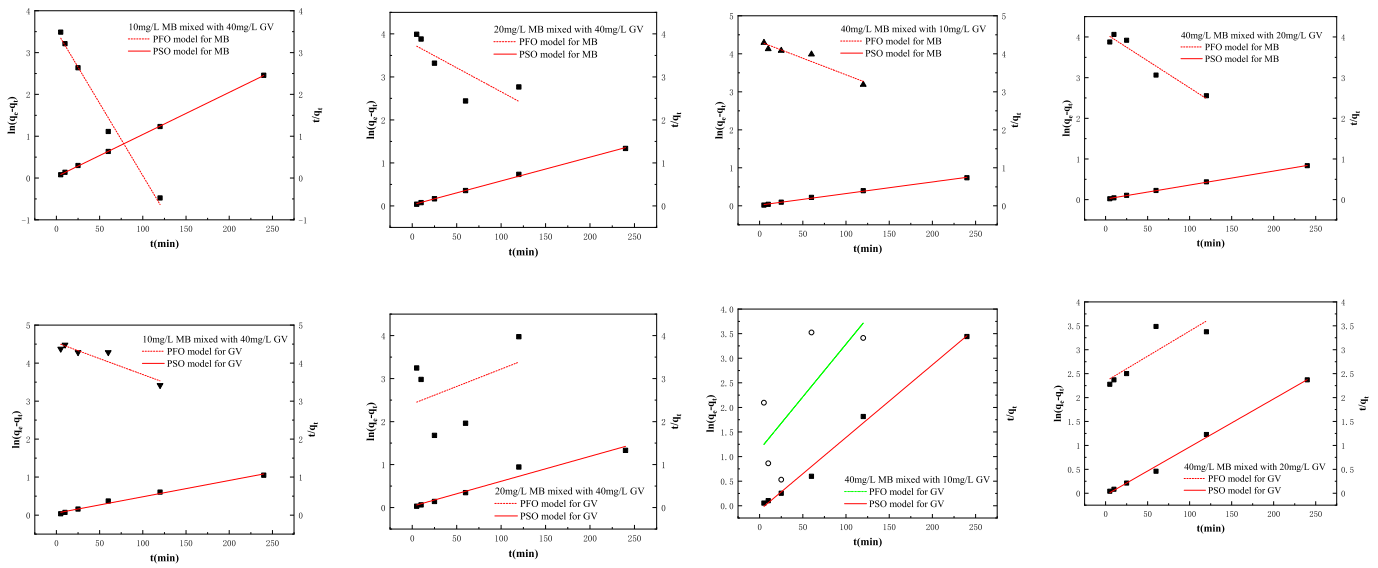


Fig. 3. PFO and PSO models plot for the adsorption of GV and MB onto SAC in two-component system.

**Table 2**  
Adsorption kinetic parameters in two-component system.

Two-component system	$q_{e,exp}$ (mg g <sup>-1</sup> )	PFO			PSO			
		$k_1$ (min <sup>-1</sup> )	$q_{e,cal}$ (mg g <sup>-1</sup> )	R <sup>2</sup>	$k_2$ (g mg <sup>-1</sup> min <sup>-1</sup> )	$q_{e,cal}$ (mg g <sup>-1</sup> )	R <sup>2</sup>	
MB(10 mg L <sup>-1</sup> ) +GV (40 mg L <sup>-1</sup> )	MB	97.68	0.0797	33.70	0.9895	3.07	99.01	0.9999
	GV	228.44	0.0193	93.43	0.8732	0.35	232.56	0.989
MB(20 mg L <sup>-1</sup> ) + GV (40 mg L <sup>-1</sup> )	MB	179.66	0.0258	43.41	0.6165	1.15	181.81	0.9981
	GV	180.37	-0.0187	11.16	0.1671	1.09	172.41	0.9591
MB(40 mg L <sup>-1</sup> ) + GV (10 mg L <sup>-1</sup> )	MB	325.15	0.0200	75.26	0.9295	0.55	322.58	0.9971
	GV	69.73	-0.0249	3.39	0.6142	-2.48	67.56	0.9929
MB(40 mg L <sup>-1</sup> ) + GV (20 mg L <sup>-1</sup> )	MB	287.73	0.0306	59.14	0.9335	0.86	294.12	0.9994
	GV	101.19	-0.0115	11.02	0.7657	-2.64	99.01	0.9962

molecule transmigration on the surface plane. Herein, this isotherm, which describes monolayer adsorption, was successfully applied to derive the best adsorption capacity. Fig. 4(a) and (b) present plots of  $C_e/q_e$  vs.  $C_e$  and their straight-line fits used to derive adsorption parameters. Specifically,  $q_m$  was obtained from the reciprocal of the slopes of these fits, while  $K_L$  values were obtained from the related intercepts. A dimensionless factor,  $R_L$  calculated by  $(1 + K_L C_i)^{-1}$  was proposed to characterize the Langmuir isotherm [37], where  $C_i$  is the initial dye concentration. The irreversible or linear adsorption can be demonstrated when  $R_L$  is equal to 0 or 1, correspondingly. Meanwhile the favorable or unfavorable adsorption is denoted by the  $R_L$  value less or greater than 1.

Multilayer adsorption of adsorbate molecules onto heterogeneous adsorbent surface can be described by the Freundlich isotherm. Fig. 4(c) and (d) present  $\ln q_e$  vs.  $\ln C_e$  plots for GV and the straight-line fits based on the Freundlich isotherms. The value of  $1/n$  was calculated from the slopes of these fits, while  $K_F$  was obtained from the related intercept. Table 3 lists the relevant parameters for MB/GV adsorption, revealing that both in the presence and absence of MB, the maximum adsorption capacity ( $q_m$ ) for GV equaled 384.61 mg g<sup>-1</sup>. This finding shows that low concentrations of MB did no significantly affect the  $q_m$  value of GV. The  $q_m$  values derived here were comparable to the reported data in Ref. [31], and the calculated  $R_L$  values less than 1 show that the adsorption of GV onto SAC is favorable.

The obtained values of  $1/n$  in the range of 0 and 1 indicate the dye adsorption ability in both single- and two-component systems.

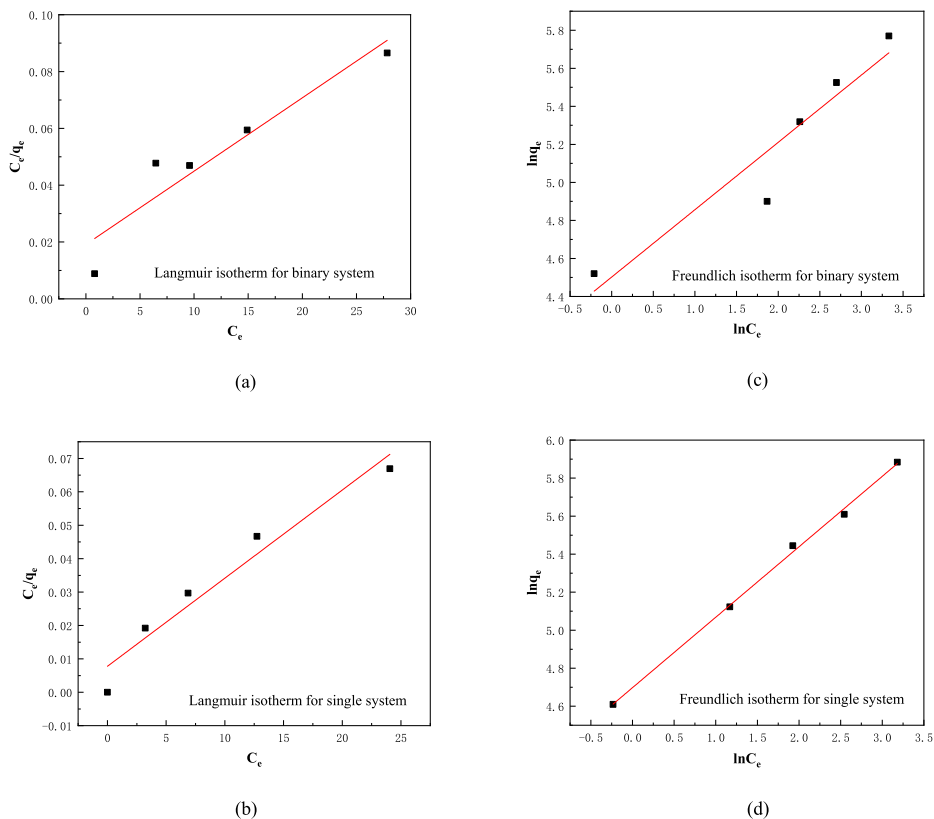


**Fig. 4.** Langmuir and Freundlich formulas plot for the adsorption of GV onto SAC in single- or two-component system.

**Table 3**  
GV adsorption isotherm parameters.

Isotherm model	Langmuir				Freundlich		
	$q_m$ (mg g <sup>-1</sup> )	$K_L$ (L mg <sup>-1</sup> )	$R^2$	$R_L$	1/n	$K_F$ (mg g <sup>-1</sup> ) (L mg <sup>-1</sup> ) <sup>1/n</sup>	$R^2$
Single-component system	384.61	0.3333	0.9504	0.0476–0.2308	0.3705	109.71	0.9978
Two-component system	384.61	0.1361	0.8951	0.1091–0.4235	0.3541	90.22	0.9093

Compared with the Langmuir isotherm, the Freundlich isotherm achieved a higher value of  $R^2$  (and thus, better described adsorption) for single-component systems, which does not consist with the findings of Regti et al. who reported that the Langmuir model would deliver the better fitting of the dyes (Basic Blue 41 and Basic Yellow 28) adsorption processes [38]. In the case of two-component systems, both the Langmuir and Freundlich isotherms featured similar values of  $R^2$ , 0.8951 and 0.9093, respectively. The low fitting correlation coefficients indicated that the competitive adsorption might occur in the two-component systems as concluded by Regti et al. [38].

### 3.5. Adsorption in two-component system

Table 4 shows the values of  $q_t$  at different times in the two-component system. At 240 min, MB adsorption capacities of 270.8 and 325.15 mg g<sup>-1</sup> were obtained for aqueous MB (40 mg L<sup>-1</sup>) without and with aqueous GV (10 mg L<sup>-1</sup>), respectively, indicating the promotional effect of GV on MB adsorption. However, when the aqueous GV (20 mg L<sup>-1</sup>) was engaged, the MB adsorption capacity declined to 287.73 mg g<sup>-1</sup>, which demonstrates the complicated processes of GV and MB simultaneous adsorption. By mixing with MB of high concentration, the GV adsorption capacity increased initially and then decreased with time, which was attributed to the strong polarity of GV and its disadvantage in terms of competitive adsorption. This phenomenon was particularly prominent for solutions of GV (10 or 20 mg L<sup>-1</sup>) mixed with MB (40 mg L<sup>-1</sup>), where GV desorption started after 60 and 5 min, respectively, and the GV adsorption capacity fluctuated with time. These results illustrate the strong competition between MB and GV adsorption. However, the MB adsorption capacity in two-component systems increased with time regardless of GV concentration, which indicated that MB exhibited better adsorption stability than GV under competitive adsorption conditions.

It is worth noting that in the GV (10 mg L<sup>-1</sup>) mixed with MB (40 mg L<sup>-1</sup>) system, the GV adsorption capacity at 60 min was close to 100 mg g<sup>-1</sup>. This indicates that GV was almost completely removed at this time, which delivered a steep reduction in adsorption mass, subsequently. Similarly, in the single-component system with only 10 mg L<sup>-1</sup> GV, the GV adsorption capacity at 240 min was also close to 100 mg g<sup>-1</sup>. This finding also showed that GV adsorption dominated the early stage, while the middle and late stages were dominated by MB adsorption.

## 4. Conclusions

The present work was focusing on the removal of dye molecules from the dyeing and printing wastewater. Aqueous GV and/or MB adsorption capacities onto SAC in the single- or two-component systems were measured to investigate the competitive adsorption mechanism. The relevant results showed that SAC had a greater adsorption capability for MB than that for GV in the single-component systems while both the adsorption processes of MB and GV could be divided into three stages based on the adsorption rate; by comparing the calculated and experimental equilibrium adsorption capacities, the better calculated values were delivered from the PSO model than those from the PFO model in single- and two-component systems; the higher fitting correlation coefficients for the single-component systems indicated that the Freundlich isotherms may describe the adsorption processes better than Langmuir isotherms meanwhile failure of the two isotherms on describe the adsorption of MB and GV in the two-component systems implied the progress of the competitive adsorption. In general, presence of GV could enhance the adsorption of MB in the binary GV-MB systems but low concentration MB in the aqueous solution did not vary the maximum adsorption capacity for GV, significantly. By investigating the adsorption mechanism thoroughly, the relevant adsorption processes and modification of adsorbent microstructure could be

**Table 4**  
Time-dependent adsorption capacity ( $q_t$ ) in two-component system.

Two-component system		$q_t$ (mg g <sup>-1</sup> )					
		5min	10min	40min	60min	120min	240min
MB(10 mg L <sup>-1</sup> ) + GV (40 mg L <sup>-1</sup> )	MB	64.94	72.82	83.70	94.64	97.06	97.68
	GV	149.04	140.06	155.93	161.83	197.91	228.44
MB(20 mg L <sup>-1</sup> ) + GV (40 mg L <sup>-1</sup> )	MB	125.48	131.2	152.01	168.21	163.75	179.66
	GV	154.63	160.69	175	173.25	127.25	180.37
MB (40 mg L <sup>-1</sup> ) + GV (10 mg L <sup>-1</sup> )	MB	251.92	263.12	265.73	271.20	300.88	325.15
	GV	91.96	97.72	98.39	100.09	66.13	69.73
MB(40 mg L <sup>-1</sup> ) + GV (20 mg L <sup>-1</sup> )	MB	239.50	229.58	237.42	266.34	274.87	287.73
	GV	120.65	119.71	118.22	130.42	97.73	101.19

manipulated specifically to improve the efficiency of decolorization of dyeing and printing wastewater.

### Author contribution

Qicheng CHEN: Conceptualization, Methodology, Funding acquisition. Qiaomu ZHANG: Data curation, Writing – original draft. Yang YANG: Methodology, Formal analysis. Qingyan WANG: Investigation, Validation. Yifeng HE: Supervision, Validation, Writing – review & editing. Nanhang DONG: Supervision, Resources, Writing – review & editing.

### Declaration of competing interest

The authors declare that they have no known competing financial interests or personal relationships that could have appeared to influence the work reported in this paper.

### Acknowledgements

This work was supported by grants from the National Natural Science Foundation of China (No. 51836001), National Key R&D Program of China (NO.2018YFB1501405) and the Jilin Provincial Special Foundation for Industrial Independent Innovation Ability, China (Grant No. 2019C026).

### References

- [1] G. Briao, S. Jahn, E. Foletto, G. Dotto, Adsorption of crystal violet dye onto a mesoporous ZSM-5 zeolite synthesized using chitin as template, *J. Colloid Interface Sci.* 508 (2017) 313–322.
- [2] Y. Liu, J.J. Lin, M.M. Chen, L. Song, Investigation on the interaction of the toxicant, gentian violet, with bovine hemoglobin, *Food Chem. Toxicol.* 58 (2013) 264–272.
- [3] J.J. McDonald, C.R. Breeden, B.M. North, R.W. Roth, Species and strain comparison of the metabolism of gentian violet by liver microsomes, *J. Agric. Food Chem.* 32 (1984) 596–600.
- [4] G.Y. Chen, S. Miao, HPLC determination and MS confirmation of malachite green, gentian violet, and their Leuco metabolite residues in channel catfish muscle, *J. Agric. Food Chem.* 58 (2010) 7109–7114.
- [5] M.T. Yagub, T.K. Sen, S. Afroze, H.M. Ang, Dye and its removal from aqueous solution by adsorption: a review, *Adv. Colloid Interface Sci.* 209 (2014) 172–184.
- [6] I. Mustafa, Methylene blue removal from water using H<sub>2</sub>SO<sub>4</sub> crosslinked magnetic chitosan nanocomposite beads, *J. Microchem.* 144 (2019) 397–402.
- [7] S.A. Al-hammadi, A.A. Al-absi, O.A. Bin-dahman, A. Saleh, Poly (trimesoyl chloride-melamine) grafted on palygorskite for simultaneous ultra-trace removal of methylene blue and toxic metals, *J. Environ. Manag.* 226 (2018) 358–364.
- [8] K. He, G. Chen, G. Zeng, A. Chen, Z. Huang, J. Shi, Journal of the Taiwan Institute of Chemical Engineers Enhanced removal performance for methylene blue by kaolin with graphene oxide modification, *J. Taiwan Inst Chem Eng.* 89 (2018) 77–85.
- [9] M. Abbas, Z. Harrache, M. Trari, Removal of gentian violet in aqueous solution by activated carbon: equilibrium, kinetics and thermodynamic study, *Adsorpt. Sci. Technol.* 37 (2019) 566–589.
- [10] D.H. Nguyen, H.N. Tran, H.P. Chao, C.C. Lin, Effect of nitric acid oxidation on the surface of hydrochars to sorb methylene blue: an adsorption mechanism comparison, *Adsorpt. Sci. Technol.* 37 (2019) 607–622.
- [11] S. Gao, W. Zhang, Z. An, S. Kong, D. Chen, Adsorption of anionic dye onto magnetic Fe<sub>3</sub>O<sub>4</sub>/CeO<sub>2</sub> nanocomposite: equilibrium, kinetics and thermodynamics, *Adsorpt. Sci. Technol.* 37 (2019) 185–204.
- [12] K. Manatura, Inert torrefaction of sugarcane bagasse to improve its fuel properties, *Case Stud. Therm. Eng.* 19 (2020) 100623.
- [13] A. Oliva, L.C. Tan, S. Papirio, G. Esposito, P.N.L. Lens, Effect of methanol-organosolv pretreatment on anaerobic digestion of lignocellulosic materials, *Renew. Energy* 169 (2021) 1000–1012.
- [14] G.B. Mensah, K.M. Darkwa, G. Laryea, Effect of combustion chamber material on the performance of an improved biomass cookstove, *Case Stud. Therm. Eng.* 21 (2020) 100688.
- [15] P. Sinuhaji, A.S. Wismogroho, G.S.T. Sinaga, I.K. Siregar, The utilization of carbonized coffee in purifying zinc dross waste by pyrometallurgy method, *Case Stud. Therm. Eng.* 17 (2020) 100576.
- [16] D. Mohan, A. Sarswat, Y.S. Ok, J.C. Pittman, Organic and inorganic contaminants removal from water with biochar, a renewable, low cost and sustainable adsorbent - a critical review, *Bioresour. Technol.* 160 (2014) 191–202.
- [17] J.A. Joseph, N. Xavier, Equilibrium and kinetic studies of methylene blue onto activated carbon prepared from crescentia cujete fruit shell, *Nat. Sci.* 11 (2013) 53–58.
- [18] N.D. Shooto, E.B. Naidoo, M. Maubane, Sorption studies of toxic cations on gingerroot adsorbent, *J. Ind. Eng. Chem.* 76 (2019) 133–140.
- [19] A.A.P. Cid, V.R. Hernandez, A.M.H. Gonzalez, A.B. Hernandez, O.C. Alonso, Synthesis of activated carbon from black sapote seeds characterized and application in the elimination of heavy metals and textile dyes, *Chin. J. Chem. Eng.* 28 (2020) 613–623.
- [20] M.P.S. Ferreira, P.S.M. Santos, M.T. Caldeira, A.C. Estrada, J.P. da Costa, T.R. Santos, A.C. Duarte, White bean (*Phaseolus vulgaris* L.) as a sorbent for the removal of zinc from rainwater, *Water Res.* 162 (2019) 170–179.
- [21] G.K. Cheruiyot, W.C. Wanyonyi, J.J. Kiplimo, E.N. Maina, Adsorption of toxic crystal violet dye using coffee husks: equilibrium, kinetics and thermodynamics study, *Sci. Afr.* 5 (2019), 00116.
- [22] J.N. Nsami, J.K. Mbadcam, The adsorption efficiency of chemically prepared activated carbon from cola nut shells by ZnCl<sub>2</sub> on methylene blue, *J. Chem. Neuroanat.* 1 (2013) 469170.
- [23] C.Y. Zhang, C.Y. Wang, G.L. Cao, W.H. Chen, S.H. Ho, Comparison and characterization of property variation of microalgal biomass with non-oxidative and oxidative torrefaction, *Fuel* 246 (2019), 375–285.
- [24] T. Onsree, N. Tippayawong, T. Williams, K. McCullough, E. Barrow, R. Pogaku, J. Lauterbach, Torrefaction of pelletized corn residues with wet flue gas, *Bioresour. Technol.* 285 (2019) 1–8.
- [25] W.Y. Han, H.H. Wang, K.D. Xi, S.S. Chen, P.X. Yan, T.S. Deng, W.B. Zhu, Superior nitrogen-doped activated carbon materials for water cleaning and energy storing prepared from renewable leather wastes, *Environ. Int.* 142 (2020) 105846.
- [26] A.E. Ofomaja, Kinetic study and sorption mechanism of methylene blue and methyl violet onto mansonia (*Mansonia altissima*) wood sawdust, *Chem. Eng. J.* 143 (2008) 85–95.
- [27] Y.D. Liang, Y.J. He, T.T. Wang, L.H. Lei, Adsorptive removal of gentian violet from aqueous solution using CoFe<sub>2</sub>O<sub>4</sub>/activated carbon magnetic composite, *J. Water Process Eng.* 27 (2019) 77–88.
- [28] J. Liu, N. Wang, H.L. Zhang, J. Baeyens, Adsorption of Congo red on Fe<sub>x</sub>Co<sub>3-x</sub>O<sub>4</sub> nanoparticles, *J. Environ. Manag.* 238 (2019) 473–483.

- [29] M. Ghaedi, N. Mosallanejad, Study of competitive adsorption of malachite green and sunset yellow dyes on cadmium hydroxide nanowires loaded on activated carbon, *J. Ind. Eng. Chem.* 20 (2014) 1085–1096.
- [30] S.S. Gupta, K.G. Bhattacharyya, Kinetics of adsorption of metal ions on inorganic materials: a review, *Adv. Colloid Interface Sci.* 162 (2011) 39–58.
- [31] I. Langmuir, The constitution and fundamental properties of solids and liquids, *J. Am. Chem. Soc.* 38 (1916) 2221–2295.
- [32] H.M.F. Freundlich, Uber die adsorption in lasungen, *J. Phys. Chem.* 57 (1906) 385–470.
- [33] A.E. Ofomaja, Intraparticle diffusion process for lead(II) biosorption onto mansonia wood sawdust, *Bioresour. Technol.* 101 (2010) 5868–5876.
- [34] A.E. Ofomaja, Kinetic study and sorption mechanism of methylene blue and methylviolet onto mansonia (*Mansonia altissima*) wood sawdust, *Chem. Eng. J.* 143 (2008) 85–95.
- [35] S.H. Chen, Q.Y. Yue, B.Y. Gao, Q. Li, X. Xu, Removal of Cr(VI) from aqueous solution using modified corn stalks: characteristic, equilibrium, kinetic and thermodynamic study, *Chem. Eng. J.* 168 (2011) 909–917.
- [36] T.S. Anirudhan, M. Ramachandran, Adsorptive removal of basic dyes from aqueous solutions by surfactant modified bentonite clay(organoclay): kinetic and competitive adsorption isotherm, *Process Saf. Environ.* 95 (2015) 215–225.
- [37] K.A.G. Gusmão, L.V.A. Gurgelb, T.M.S. Melo, L.F. Gil, Application of succinylated sugarcane bagasse as adsorbent to remove methylene blue and gentian violet from aqueous solutions - kinetic and equilibrium studies, *Dyes Pigments* 92 (2012) 967–974.
- [38] A. Regti, A. El Kassimi, M.R. Laamari, M.E. Haddad, Competitive adsorption and optimization of binary mixture of textile dyes: a factorial design analysis, *Journal of the Association of Arab Universities for Basic and Applied Sciences* 24 (2017) 1–9.